

Interaction of dissipative solitons stabilized by nonlinear gradient termsOrazio Descalzi ^{1,2,*}, Carlos Cartes,¹ and Helmut R. Brand ²¹*Complex Systems Group, Facultad de Ingeniería y Ciencias Aplicadas, Universidad de los Andes, Santiago 7620001, Chile*²*Department of Physics, University of Bayreuth, 95440 Bayreuth, Germany* (Received 6 October 2020; revised 18 February 2021; accepted 2 April 2021; published 30 April 2021)

We study the interaction of stable dissipative solitons of the cubic complex Ginzburg-Landau equation which are stabilized only by nonlinear gradient terms. In this paper we focus for the interactions in particular on the influence of the nonlinear gradient term associated with the Raman effect. Depending on its magnitude, we find up to seven possible outcomes of these collisions: Stationary bound states, oscillatory bound states, meandering oscillatory bound states, bound states with large-amplitude oscillations, partial annihilation, complete annihilation, and interpenetration. Detailed results and their analysis are presented for one value of the corresponding nonlinear gradient term, while the results for two other values are just mentioned briefly. We compare our results with those obtained for coupled cubic-quintic complex Ginzburg-Landau equations and with the cubic-quintic complex Swift-Hohenberg equation. It turns out that both meandering oscillatory bound states as well as bound states with large-amplitude oscillations appear to be specific for coupled cubic complex Ginzburg-Landau equations with a stabilizing cubic nonlinear gradient term. Remarkably, we find for the large-amplitude oscillations a linear relationship between oscillation amplitude and period.

DOI: [10.1103/PhysRevE.103.042215](https://doi.org/10.1103/PhysRevE.103.042215)**I. INTRODUCTION AND MOTIVATION**

Collisions of dissipative solitons (DSs) can be found in the literature in fields ranging from hydrodynamics to chemical reactions on surfaces including biological media and fiber lasers in optics [1–7]. DSs are spatially localized objects appearing in dissipative driven pattern-forming nonequilibrium systems along with nonlinearity and dispersion [8]. In the CO oxidation reaction on Pt(110), in some cases, solitary waves that preserve their shapes and speed after collisions have been observed (interpenetration), but collisions lead mostly to mutual annihilation [1] while in collisions of subsurface oxygen waves fragments the thicker one takes over the thinner one (partial annihilation) [2]. Soliton-like behavior has also been observed in the electro-oxidation of CO in Pt [3]. In hydrodynamics, in an annular thin layer of a binary mixture heated from below, the collision of counterpropagating confined states has been studied. Partial annihilation (only one pulse survives the collision) and bound states arise for high and low approach velocities, respectively [4,5]. Solitonic behavior has also been reported for the mass cell movement of nonchemotactic mutants of the cellular slime mould *Dictyostelium discoideum* [6]. In optics it has been revealed that the collision of pulses can induce explosions in a mode-locked fiber laser [7].

From a theoretical point of view, interpenetration between pulses as well as bound states, mutual and partial annihilation have been studied in pioneering works using counterpropagating coupled complex cubic-quintic Ginzburg-Landau equations (CQGLEs). The result was that, in one spatial dimension (for negative linear dispersion and negative

real part of the coupling), collisions of counterpropagating pulses can lead, in particular, to complete interpenetration or annihilation [9]. Interactions of pulses which breathe in the modulus lead to interpenetration, annihilation and partial annihilation [10].

An effort to understand the phenomenon of partial annihilation in coupled complex CQGLEs (for the collision of stationary pulses) has been carried out by introducing additive noise to the equation near the boundaries between different outcomes. We concluded that a small amount of noise can induce partial annihilation of colliding dissipative solitons [11]. Recently, we have shown that for a large range of approach velocities and stabilizing cubic-cross couplings two stationary counterpropagating pulses can undergo partial annihilation via a spontaneous breaking of symmetry [12].

The complex CQGLE is a prototype envelope equation arising at the onset of a weakly inverted instability against traveling waves [13,14]. The advantage of using this equation is that it has stable pulse solutions, inside the range of parameters where two homogeneous attractors coexist, due to a nonvariational feedback mechanism between the amplitude and the frequency, and a saddle-node instability giving rise to a pair of pulses (stable and unstable) [15].

Collisions of localized solutions have also been studied in the framework of order parameter equations. In the one-dimensional quintic Swift-Hohenberg equation with complex coefficients, in particular, it has been found that the head-on collision of two stable localized traveling states results in the formation of a localized standing wave pattern and that two counterpropagating localized traveling states can interpenetrate [16].

A different theoretical approach to the study of collisions of dissipative solitons are reaction-diffusion equations. Soliton-like behavior and annihilation has been observed in

*Corresponding author: odescalzi@miuandes.cl

a model of the Belousov-Zhabotinsky (BZ) reaction [17], in the Bonhoeffer van der Pol reaction-diffusion system [18,19], and in the FitzHugh-Nagumo system [20]. Experiments and modeling have been carried out for the CO oxidation on Pt [2,3]. In a simple model for the same reaction, assuming structural imperfections, it has been shown that soliton-like behavior and partial annihilation can arise [21].

The inclusion of nonlinear gradient terms in single and coupled complex CQGLEs deserves a special place in this introduction. Nonlinear gradients occur to the same order as the quintic terms [13,14]. These terms might or not be important depending on the physics of the system. In a pioneering work, these terms were investigated in connection with binary fluid convection, which resulted in a reduction of the group velocity and asymmetry of the pulses [22]. Subsequently, the effects of nonlinear gradient terms on breathing pulses were studied [23].

In optics, when modeling a nonlinear fiber for ultrashort pulses, it can be necessary to include higher-order nonlinear and dispersive effects, such as intrapulse Raman scattering, self-steepening, and third-order dispersion [24–26].

Recently, Facao and Carvalho have published a series of articles showing that the complex cubic Ginzburg-Landau equation (CGLE) together with nonlinear gradients can lead to stable moving pulses with a fixed or oscillating shape [27–29]. It is worth noting here that the complex CGLE [30] (without quintic nonlinearities) has only unstable pulses.

This new mechanism of stabilization of pulses is added to the others already known: The nonvariational feedback mechanism between the amplitude and the frequency, already mentioned above [15]; spatially localized regions in wavelength, in the framework of nonlinear phase dynamics [31–33]; coupling between an envelope equation for an oscillatory instability and a phase equation [34,35]; and the trapping mechanism, where the slowly varying pattern amplitude becomes trapped by the rapid spatial variations [16,36].

Recently, we have shown that the existence of stable moving pulses in the complex CGLE with nonlinear gradients can be understood by a continuous supply and dissipation of energy in the framework of a mechanical analog [37,38]. This picture has been useful in the analysis of the stabilization mechanism demonstrating that all terms of the equation are essential.

In the present paper we study the interaction of stable DSs of the cubic complex Ginzburg-Landau equation which are stabilized exclusively by nonlinear gradient terms (NLGS DSs). We focus for the interactions in particular on the influence of the Raman term. Depending on the magnitude of the Raman term, we find up to seven possible outcomes of these collisions. We compare our results with those obtained for coupled cubic-quintic complex Ginzburg-Landau equations and with the cubic-quintic complex Swift-Hohenberg equation.

The paper is organized as follows. In Sec. II we summarize the ingredients of the equations studied and the numerical methods used. In Sec. III we characterize in detail the results and analyze the consequences. In Sec. IV we describe transitions between patterns and some of their specific properties and in Sec. V we present conclusions and perspectives.

II. THE MODEL

We consider in a nonlinear fiber a wave packet centered at the wave number k_0 and frequency ω_0 . All wave numbers close to k_0 satisfy $k = \omega n(\omega)/c$ that is $k = k(\omega)$, and $n(\omega)$ the refractive index. The wave packet is modulated by an envelope Ψ , which depends on the slow space X and the slow time T . W is a wave moving to the right,

$$W = \text{Re}[\Psi(X, T)e^{ik_0x - i\omega_0t}]. \quad (1)$$

Thus we can make a formal expansion around k_0 : $k - k_0 = (\frac{\partial k}{\partial \omega})(\omega - \omega_0) + \frac{1}{2}(\frac{\partial^2 k}{\partial \omega^2})(\omega - \omega_0)^2 + \dots$, where $\frac{\partial k}{\partial \omega}$ evaluated at ω_0 corresponds to $1/v_g$, that is the inverse of the group velocity of the wave packet, and $\frac{\partial^2 k}{\partial \omega^2} \equiv \beta_2$ is the group velocity dispersion ($\beta_2 < 0$, anomalous dispersion). Setting $k - k_0 = K$ and $\omega - \omega_0 = \Omega$ we obtain a dispersion relation for the envelope Ψ ,

$$K = \frac{1}{v_g}\Omega + \frac{1}{2}\beta_2\Omega^2 + \dots \quad (2)$$

The response of any dielectric medium to an intense electromagnetic field E becomes nonlinear leading to a refractive index of the form $n(\omega, |E|^2) = n_0(\omega) + n_2|E|^2$, where n_2 is the Kerr coefficient. By incorporating in the above dispersion relation (2) the Kerr effect, fiber losses ($\delta < 0$), nonlinear gain of energy $\epsilon > 0$, and the curvature of the frequency response of the narrow-band filter ($\beta > 0$) we obtain the complex CGLE. For a wide spectrum (>0.1 THz) energy can be transferred from the high-frequency components to the low-frequency ones, phenomenon called intrapulse Raman scattering [24]. Nevertheless, for pulses wide enough containing many cycles (~ 100 fs = 0.1 ps) the complex CGLE considering self-steepening (S_r) and delayed Raman response (R_r) reads

$$i\left[\partial_X\Psi + \frac{1}{v_g}\partial_T\Psi\right] - \frac{1}{2}\beta_2\partial_T^2\Psi + |\Psi|^2\Psi - i\delta\Psi - i\epsilon|\Psi|^2\Psi - i\beta\partial_T^2\Psi = R_r\Psi\partial_T(|\Psi|^2) - iS_r\partial_T(|\Psi|^2). \quad (3)$$

Facao and Carvalho, in a recent series of articles [27–29], studied Eq. (3) and its generalizations, without group velocity, and showed that this equation admits, in particular, moving stable pulses for the following combinations: $R_r \neq 0$ and $S_r = 0$; $R_r = 0$ and $S_r \neq 0$; and $R_r \neq 0$, $S_r \neq 0$. However, in this article we will focus only on the case $R_r \neq 0$, $S_r = 0$. It is important to emphasize that the cubic complex Ginzburg-Landau equation without quintic nonlinearities or nonlinear gradient terms has only unstable pulses.

The velocity of the pulses $v(R_r)$ is constant (without considering the group velocity). This and the shape (asymmetric) of the pulses depend, in particular, on the magnitude and sign of the parameter R_r .

Recently we have shown that the velocity $v(R_r)$ satisfies a hyperbola over a large range of R_r values [37], that is, $v(R_r) \sim 1/R_r$. Thus the total velocity of the pulse is $v_g + v(R_r)$.

An equivalent equation to Eq. (3) is the cubic complex Ginzburg-Landau equation for the envelope of linear unstable modes at the onset of a subcritical oscillatory instability

considering nonlinear gradients and group velocity

$$\begin{aligned} \partial_t A + v_g \partial_x A &= \mu A + (\beta_r + i\beta_i)|A|^2 A \\ &\quad - iR_r A \partial_x (|A|^2) + (D_r + iD_i) \partial_x^2 A, \end{aligned} \quad (4)$$

where we have discarded self-steepening S_r .

In this paper we investigate the collision of pulses by means of two coupled complex cubic Ginzburg-Landau equations with nonlinear gradient terms and group velocities for counterpropagating waves:

$$\begin{aligned} \partial_t A + v_g \partial_x A &= \mu A + (\beta_r + i\beta_i)|A|^2 A \\ &\quad + iR_r (|A|^2)_x A + (c_r + ic_i)|B|^2 A \\ &\quad + (D_r + iD_i) \partial_x^2 A, \end{aligned} \quad (5)$$

$$\begin{aligned} \partial_t B - v_g \partial_x B &= \mu B + (\beta_r + i\beta_i)|B|^2 B \\ &\quad - iR_r (|B|^2)_x B + (c_r + ic_i)|A|^2 B \\ &\quad + (D_r + iD_i) \partial_x^2 B, \end{aligned} \quad (6)$$

where $A(x, t)$ and $B(x, t)$ are complex fields and where we have considered cubic cross-coupling terms.

In optics [Eq. (3)] R_r must be positive, while for envelope equations [Eqs. (5) and (6)], of more general applications, deduced close to a weakly inverted bifurcation to an oscillatory instability this is not necessary, and thus the net velocity for the right moving pulse should be $v = v_g - v(R_r)$. In optics the group velocity depends on the frequency ω_o of the carrier wave. We emphasize that for envelope equations as they arise near a weakly inverted bifurcation associated with an oscillatory instability, nonlinear gradient terms arise naturally to lowest consistent order in the distance from onset [13,14]. We also note that the approach velocity of colliding DSs can be changed experimentally, for example, near convective onset in miscible binary fluid mixtures by changing the separation ratio (or Soret effect) [4,5] or for autocatalytic surface reactions [2] by changing parameters such as pressure, temperature, and the concentration of the participating gases.

We have carried out our numerical studies for the following values of the parameters, which we kept fixed for the present purposes: $\mu = -0.012$, $\beta_r = 0.3$, $\beta_i = 1.0$, $c_i = 0$, $D_r = 0.6$, and $D_i = 0.5$. Positive values of D_i correspond to the regime of anomalous linear dispersion and are necessary to obtain stable NLGS DSs in the present case. We also note that the chosen value of μ is only weakly subcritical. Time integration of Eqs. (5) and (6) was performed using fourth-order Runge-Kutta finite differencing. We took as a time step $dt = 0.002$ and a grid spacing of $dx = 0.05$ leading to a box size of $L = 62.5$ for $N = 1250$ data points. The time step and the grid spacing were varied by a factor of 3 to study the effects of discretization. The values used are a compromise between accuracy and required runtime. None of the results reported depends sensitively on the box size.

III. RESULTS AND DISCUSSION FOR THE INTERACTION OF NLGS DSs

We were running three values of R_r to investigate the outcome of collisions: $R_r = 0.2$, $R_r = 0.4$, and $R_r = 0.1$. It turned out that the values $R_r = 0.1$ and $R_r = 0.2$ give

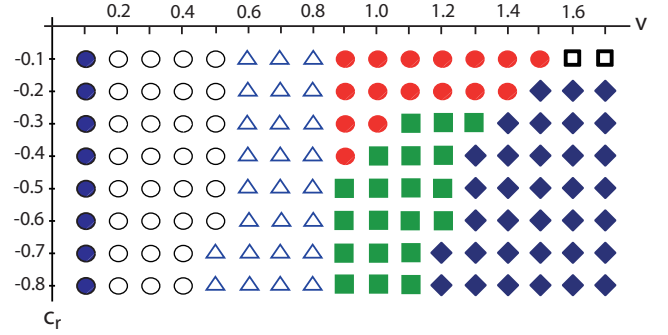


FIG. 1. Phase diagram of possible outcomes of collisions of stationary NLGS DSs for $R_r = 0.1$ plotted as c_r versus velocity v . Filled black circles (\bullet) indicate stationary bound states, open black circles (\circ) oscillatory bound states, open blue triangles meandering oscillatory bound states (Δ), red solid circles partial annihilation (\bullet), green solid squares large-amplitude oscillatory bound states (\blacksquare), blue diamonds annihilation (\blacklozenge), and black open squares (\square) interpenetration. The parameters are as follows: $\mu = -0.012$, $\beta_r = 0.3$, $\beta_i = 1.0$, $D_r = 0.6$, and $D_i = 0.5$.

rise to a large number of possible outcomes of collisions varying the approach velocity and the stabilizing value of the cross-coupling c_r . For $R_r = 0.4$ the number of outcomes is considerably reduced but predominantly includes annihilation, interpenetration, and oscillatory bound states. Throughout the rest of this paper we concentrate on the results for $R_r = 0.1$ and their discussion.

In the phase diagram Fig. 1 we plot the outcome of collisions for interacting DSs with the Raman nonlinear gradient term. The parameters varied to obtain the plot are the approach velocity and the stabilizing cross-coupling c_r between counterpropagating DSs. As a result of the collisions we obtain stationary bound states, oscillatory bound states, meandering oscillatory bound states, large-amplitude oscillatory bound states, partial annihilation, annihilation, and interpenetration.

The run time used to obtain the phase diagram shown in Fig. 1 was $T = 400$ and the timescale of the $x-t$ plots shown below varies between $T = 30$ and $T = 360$ to elucidate the important features of the interaction and/or the characteristic features of the asymptotic state. In the $x-t$ plots we always incorporate both the asymptotic regime as well as the initial conditions. We note that the scales in x and t on all $x-t$ plots shown are linear.

For the initial condition we prepared two NLGS DSs located around $x_1 = 12.5$ and $x_2 = 50$ symmetrically with respect to $x = 31.25$ for the initial approach of the two dissipative solitons. For the cases of stationary bound states, oscillatory bound states, annihilation and interpenetration this high degree of symmetry in the $x-t$ plots is also maintained throughout the whole time evolution shown.

In Ref. [12] we have also demonstrated that for the case of partial annihilation this symmetry is maintained on average for partial annihilation when the processes of partial annihilation moving to the right and partial annihilation moving to the left are compared.

Starting with a small approach velocity, we obtain first stationary bound states (Fig. 2) followed by slightly higher

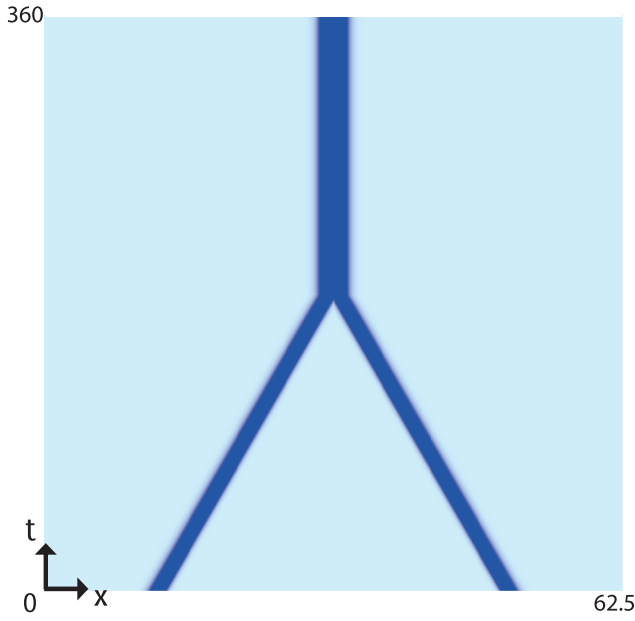


FIG. 2. The x - t plot of $\text{Max}(|A|, |B|)$ showing the temporal generation of a stationary bound state indicated by the black solid circles in Fig. 1 for $c_r = -0.3$ and $v = 0.1$. The timescale shown is $T = 360$ and the box size $L = 62.5$.

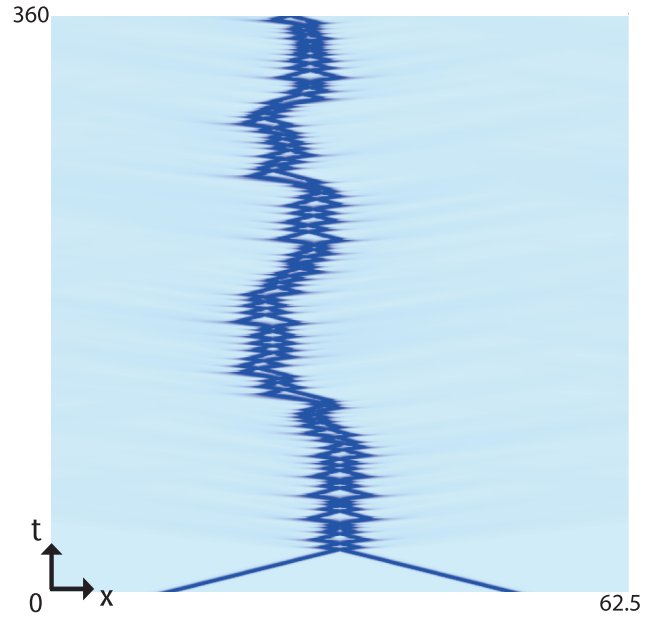


FIG. 4. The x - t plot of $\text{Max}(|A|, |B|)$ showing the time evolution of a meandering oscillatory bound state indicated by the open blue triangles in Fig. 1 for $c_r = -0.5$ and $v = 0.7$. The timescale shown is $T = 360$ and the box size $L = 62.5$.

approach velocity by oscillatory bound states (Fig. 3) over the whole range of the stabilizing cross-coupling c_r studied. As the approach velocity is increased to $v \sim 0.6$, a meandering oscillatory bound state of the type depicted in Fig. 4 results. One clearly sees fairly large excursions of the oscillations to the left and to the right in a rather irregular fashion. In addition, the amplitude of the phonon shedding increases.

A further increase of the approach velocity v leads, for fixed v and varying c_r , to two different outcomes. For smaller values of c_r (that is for more stabilizing cross-coupling) we find large-amplitude oscillatory bound states plotted in Fig. 5. In Fig. 6 we have plotted four snapshots of the large-amplitude oscillatory bound state during one period, T , equally distant in time ($T/4$). Clearly the NLGS DS becomes narrower and higher as well as broader and lower as a function of time in an alternating fashion.

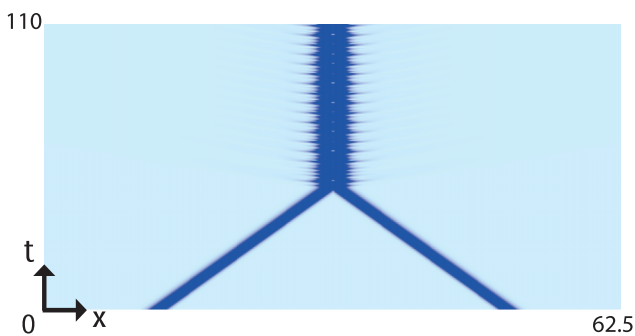


FIG. 3. The x - t plot of $\text{Max}(|A|, |B|)$ showing the temporal generation of an oscillatory bound state indicated by the black open circles in Fig. 1 for $c_r = -0.3$ and $v = 0.4$. The timescale shown is $T = 110$ and the box size $L = 62.5$.

To characterize the meandering oscillatory bound states we have analyzed time-series and Fourier spectra. In Fig. 7 we have plotted two independent time series for the integral $I_A(t) \equiv \int |A(x, t)| dx$ for meandering oscillatory bound

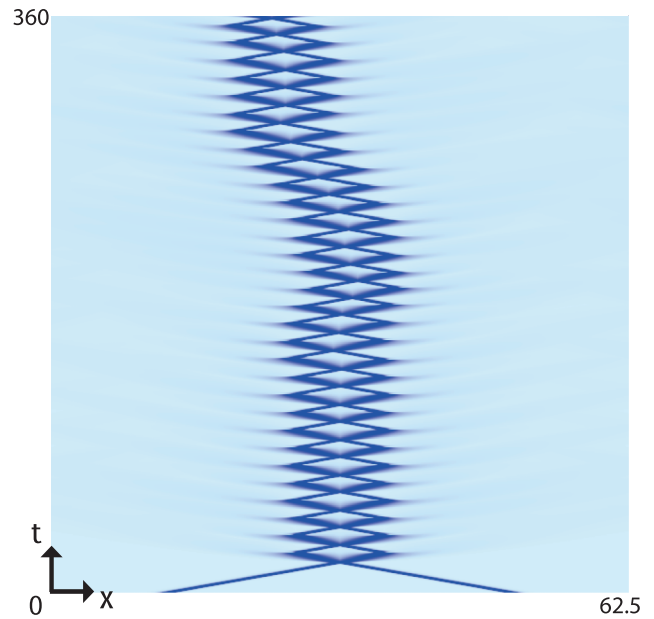


FIG. 5. The x - t plot of $\text{Max}(|A|, |B|)$ showing the time evolution of a large-amplitude oscillatory bound state indicated by the green solid squares in Fig. 1 for $c_r = -0.5$ and $v = 1.0$. The timescale shown is $T = 360$ and the box size $L = 62.5$. We note that the large-amplitude oscillations are combined with some degree of meandering on timescales large compared to the frequency of the oscillations.

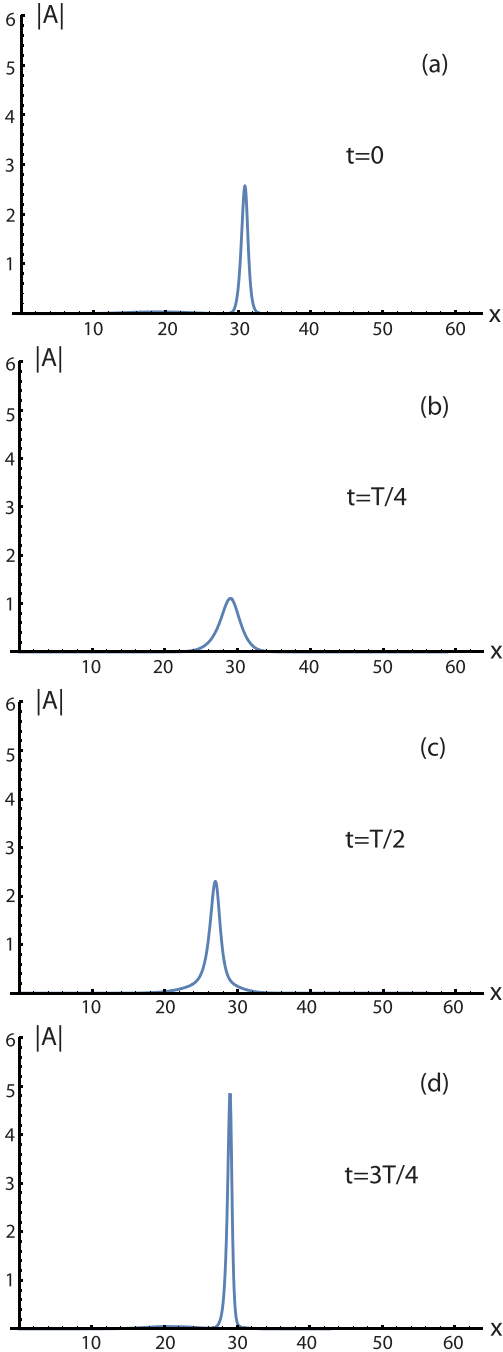


FIG. 6. Four snapshots of $|A|$ as a function of space x during one period T and plotted $T/4$ apart for the large-amplitude oscillatory bound state; $c_r = -0.5$ and $v = 1.0$.

states for $c_r = -0.5$ and $v = 0.7$ starting with very similar initial conditions and pointing to chaotic behavior as revealed by the rather different time-dependent behavior for longer times. This point is further corroborated by the Fourier spectra $S(\omega) = |u(\omega)|^2$, where

$$u(\omega) = \int_{-\infty}^{\infty} I_A(t) e^{-i\omega t} dt \quad (7)$$

and $S(0) = 0$, shown in Fig. 8 for meandering oscillatory bound states on top ($c_r = -0.5$ and $v = 0.7$) and for large-

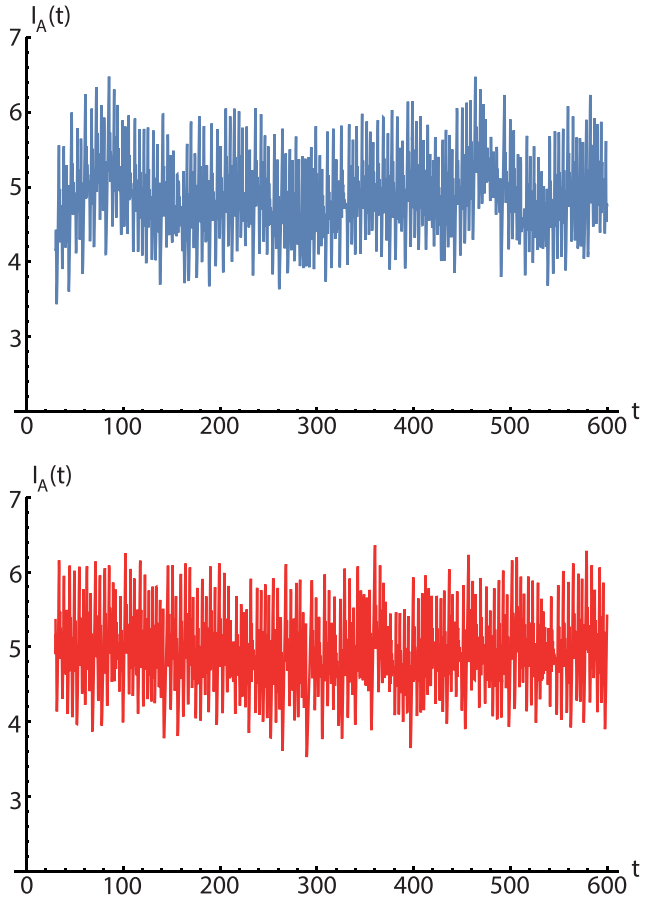


FIG. 7. Two time series of the quantity $I_A(t) \equiv \int |A(x, t)| dx$ are shown for the meandering oscillatory bound state for $c_r = -0.5$ and $v = 0.7$ from $t = 30$ to $t = 600$.

amplitude oscillatory bound states at the bottom ($c_r = -0.5$ and $v = 1.0$). We have used the convention $S(0) = 0$ to improve the visualization of the spectra; its only effect is to remove the constant part from $I_A(t)$. From Fig. 8 bottom we extract a fundamental ω value of $\omega \approx 0.57$ corresponding to a frequency f , $f = \frac{\omega}{2\pi} \approx 0.0907$. This value compares well with the frequency deduced from Fig. 15, where we have $T = 11.1$ leading to $f = 0.0900$. Clearly meandering oscillatory bound states reveal a Fourier spectrum characteristic of chaotic behavior, while large-amplitude oscillatory bound states are essentially periodic in nature.

For larger values of c_r and $v = 1.0$ partial annihilation after a fairly long interaction time results (Fig. 9). We note that in the case of partial annihilation the rather long interaction is associated with temporal oscillations of shrinking amplitude until a dissipative NLGS DS moving to the right (in the case shown) emerges. Naturally DSs moving to the right and to the left arise equally frequently on average. An example of both types of behavior has already been elucidated in Ref. [12].

A further increase in the approach velocity leads for $|c_r| \gtrsim 0.2$ to complete annihilation shown in Fig. 10. We note that, in contrast to the case of partial annihilation depicted in Fig. 9, the interaction time is rather short. For small values of $|c_r|$ we obtain interpenetration after a fairly short interaction time (Fig. 11). This outcome is to be expected intuitively,

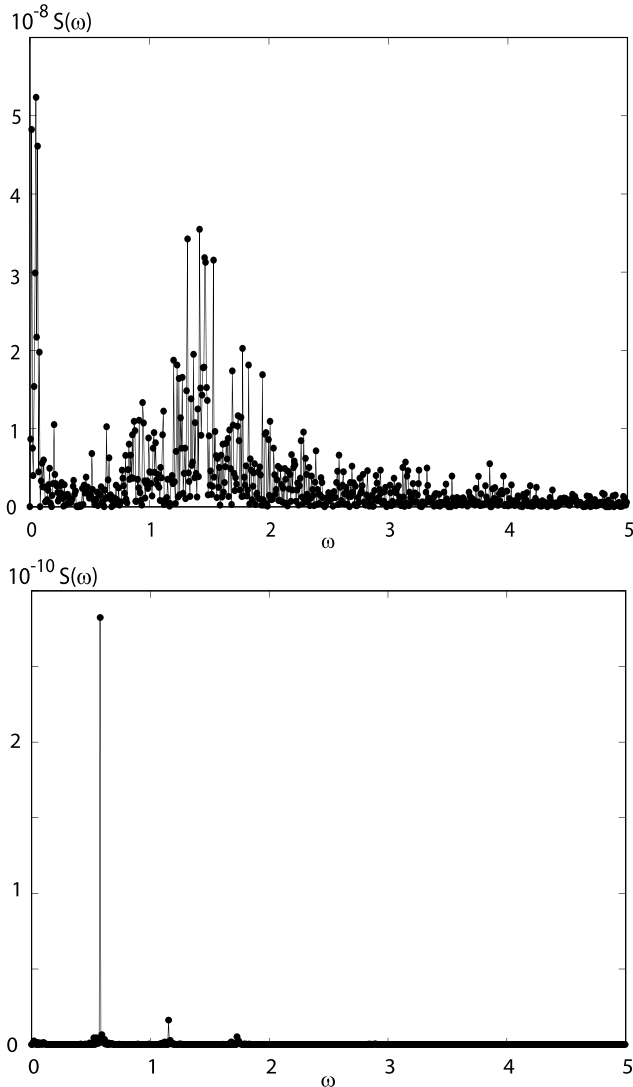


FIG. 8. The Fourier spectra $S(\omega)$ for meandering oscillatory bound states ($c_r = -0.5$ and $v = 0.7$) (top) and for large-amplitude oscillatory bound states ($c_r = -0.5$ and $v = 1.0$) (bottom) are plotted for comparison. The range covered for ω is $0 \leq \omega \leq 5$. We note the change of scale on the ordinate. While the spectrum for the meandering oscillatory bound state is clearly showing signatures of chaotic behavior, the spectrum for the large-amplitude oscillatory bound state shows predominantly periodic behavior with the fundamental and the first few harmonics.

since in the limit $|c_r| \rightarrow 0$ there is no interaction between DSs propagating to the left and to the right, respectively.

Since the interaction of NLGS DSs has not been studied before, it appears to be instructive to compare the results presented here to those obtained so far for other experimental and theoretical pattern-forming dissipative systems. First, we briefly sketch the experimental situation. When it comes to interpenetration (soliton-like behavior), such observations have been obtained in surface reactions [1], genetically modified biological systems [6], and electro-oxidation on surfaces [3]. Partial annihilation has been reported mainly for surface reactions [1,2] and near convective onset in binary fluid mixtures

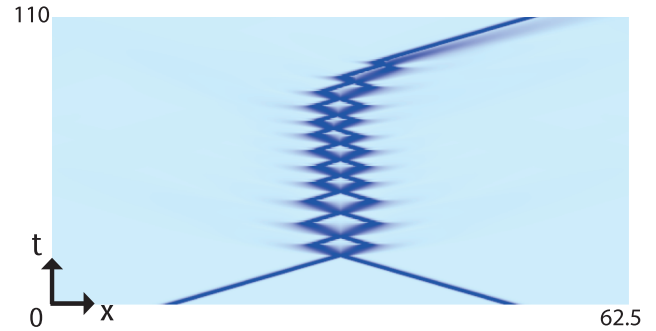


FIG. 9. The $x-t$ plot of $\text{Max}(|A|, |B|)$ showing the partial annihilation indicated by the red solid circles in Fig. 1 for $c_r = -0.3$ and $v = 1.0$. The $x-t$ plot includes both the initial approach and the temporal behavior after the partial annihilation is completed. The timescale shown is $T = 110$ and the box size $L = 62.5$.

[4,5]. By comparison stationary bound states appear to be comparatively rare but have been thoroughly characterized near convective onset in binary fluid mixtures.

On the modeling side there is a large body of literature studying coupled complex cubic-quintic complex Ginzburg-Landau equations as they emerge as envelope equations near onset of a weakly inverted bifurcation to traveling waves. Focusing on one dimensional situations, the present state can be summarized as follows. Stationary bound states, interpenetration and complete annihilation have been studied in Refs. [9] and [22], while partial annihilation has been investigated in Refs. [11,12]. Oscillatory bound states after the collision of two stationary DSs have been identified in Refs. [39,40]. We also note that stationary bound states and interpenetration of stationary DSs have been found for the cubic-quintic complex Swift-Hohenberg equation [16].

We thus arrive at the conclusion that, while a number of outcomes of collisions of stationary DSs have been observed before for coupled cubic-quintic CGL equations and for the cubic-quintic complex Swift-Hohenberg equation, several results of such collisions appear specifically for colliding stationary NLGS DSs: Meandering oscillatory bound states as well as large-amplitude oscillatory bound states. We speculate that these two new classes of outcome are associated with the

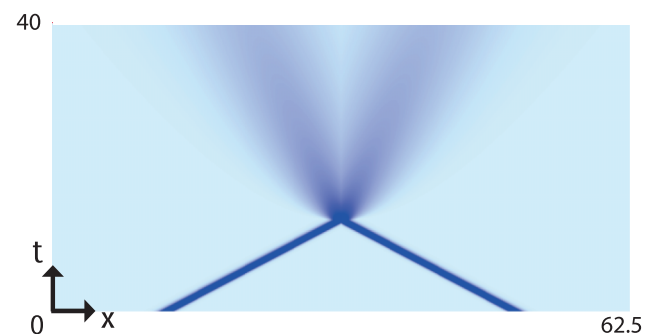


FIG. 10. The $x-t$ plot of $\text{Max}(|A|, |B|)$ showing the annihilation indicated by the blue solid diamonds in Fig. 1 for $c_r = -0.3$ and $v = 1.5$. The $x-t$ plot includes both the initial approach and the temporal behavior after the annihilation is completed. The timescale shown is $T = 40$ and the box size $L = 62.5$.

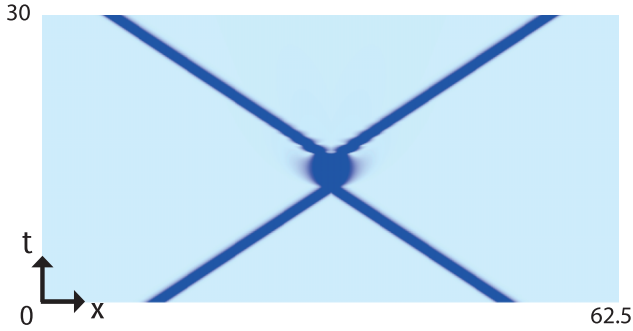


FIG. 11. The x - t plot of $\text{Max}(|A|, |B|)$ showing the process of interpenetration indicated by the open black squares in Fig. 1 for $c_r = -0.1$ and $v = 1.6$. The x - t plot includes both the initial approach and the temporal behavior after the annihilation is completed. The timescale shown is $T = 30$ and the box size $L = 62.5$.

fact that NLGS DSs are solely stabilized by a cubic nonlinear gradient term.

IV. DETAILED CHARACTERIZATION OF SELECTED PATTERNS FORMED AND THEIR TRANSITIONS

A. The transition from stationary bound states to oscillatory bound states

To investigate the transition from stationary bound states to oscillatory bound states in detail we have analyzed time series of the integral $I_A(t) \equiv \int |A(x, t)| dx$. We found that for $v < v_c$, $I_A(t) = I_0 \text{const.}$ For $v \geq v_c$, $I_A(t) = I_0 + \frac{R}{2} e^{i\Omega_H t + i\phi_0} + \text{c.c.}$ at the onset of the oscillatory instability. In Fig. 12 we see that for $c_r = -0.5$ and for the interval of velocities $0.10 \leq v \leq 0.20$ the oscillation amplitude R shows a growth behavior of the type $R = 0.68\sqrt{v - v_c}$ with $v_c = 0.104$.

Therefore, the normal form describing the transition at the onset of the Hopf bifurcation can be formulated as

$$\psi_t = (v - v_c + i\Omega_H)\psi - (\alpha_r + i\alpha_i)|\psi|^2\psi. \quad (8)$$

Setting $\psi = R e^{i\omega t + i\phi_0}$, we obtain $R = \sqrt{(v - v_c)/\alpha_r}$. Thus α_r can be obtained as $\alpha_r = 2.16$. To check further the consistency with Eq. (8), we have plotted ω , the frequency of the oscillatory bound states obtained from Fourier transforms, in Fig. 12(c). The best fit is a straight line as expected for a Hopf bifurcation

$$\omega = \Omega_H - (v - v_c) \frac{\alpha_i}{\alpha_r}. \quad (9)$$

This result underscores the picture of a forward Hopf bifurcation for the transition from stationary bound states to oscillatory bound states. From Eq. (9) and Fig. 12(c) we obtain $\alpha_i = 7.97$ and $\Omega_H = 5.78$.

B. The transition to chaotic behavior in the regime of oscillatory bound states

As a remarkable feature we find a transition to chaos within the regime of oscillatory bound states. In Fig. 13 we have plotted the first steps of the transition to chaos: Figure 13(a) shows the state before a first doubling of the period for $v = 0.22$ followed by Fig. 13(b) at the transition to the first doubling

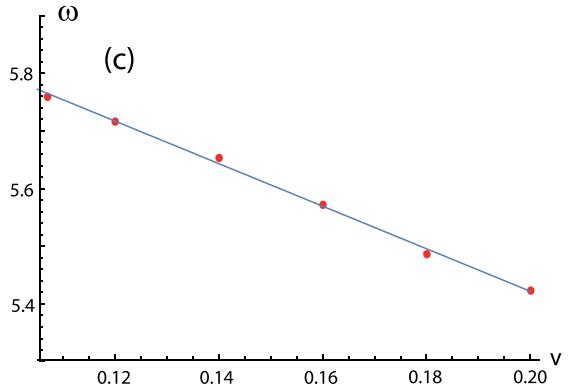
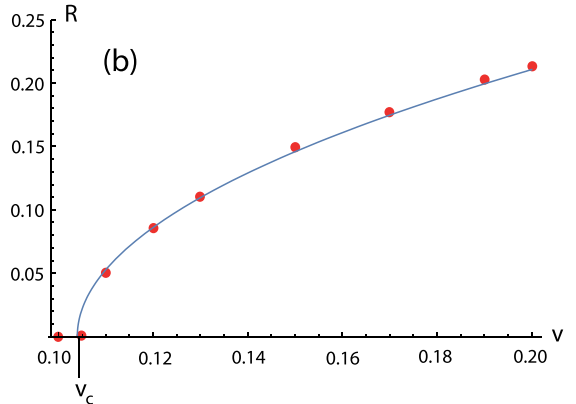
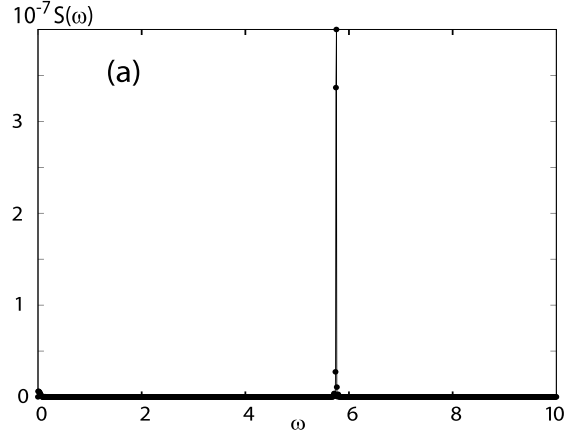


FIG. 12. Transition from a stationary bound state to oscillatory bound states. $c_r = -0.5$. (a) Fourier spectrum giving rise to $\omega = 5.76$ for $v = 0.11$; (b) amplitude R as a function of v demonstrating that it is a Hopf bifurcation $R \sim (v - v_c)^\gamma$ with $v_c = 0.104$ and an exponent $\gamma = 0.50$; (c) ω is plotted as a function of v and fitted to a straight line as predicted by Eq. (8).

with the new amplitudes still fairly small at $v = 0.23$. In Fig. 13(c) for $v = 0.24$ the first period doubling is completed with a fairly large amplitude for the doubled period. In Fig. 14 we summarize the Fourier spectra for larger values of the velocity, v . At $v = 0.30$ [Fig. 14(a)] the next period doubling occurs. At $v = 0.315$ additional frequencies enter the picture [Fig. 14(b)]. For $v = 0.40$ a fully developed chaotic state is obtained [Fig. 14(c)]. To further analyze the results from the

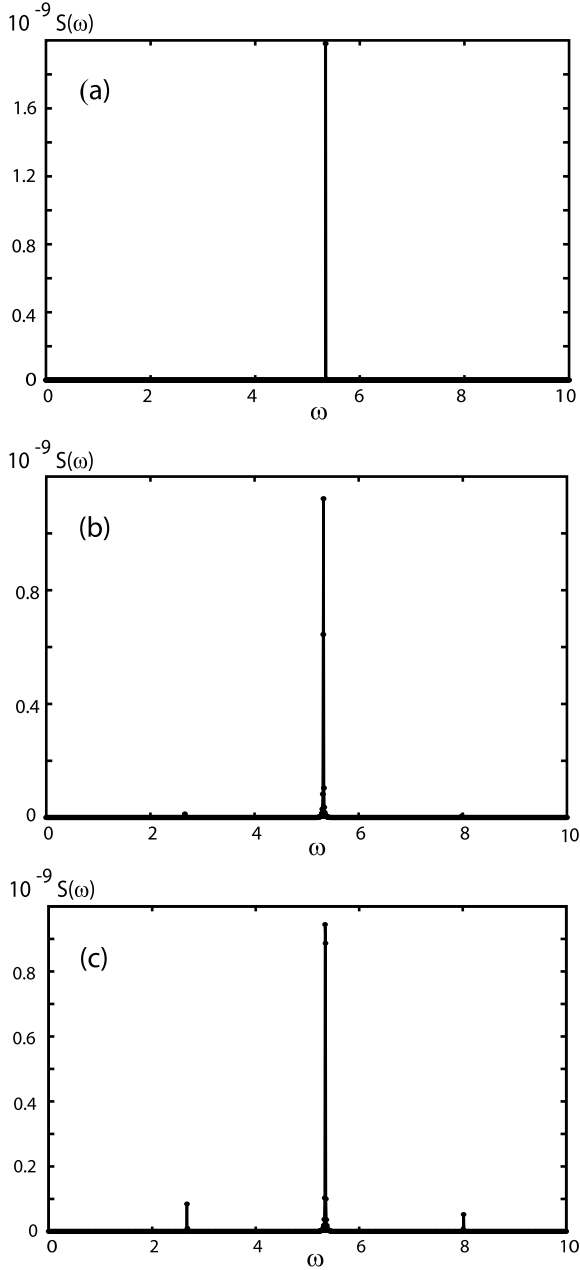


FIG. 13. In this plot we show the first period doubling in the regime of oscillatory bound states for $c_r = -0.5$. The Fourier spectra are for three values of the velocity v : (a) $v = 0.22$, the state before the first period doubling; (b) $v = 0.23$, at the transition to the first period doubling, with the new amplitude still fairly small; and (c) $v = 0.24$ first period doubling completed with fairly large amplitude for the doubled period.

Fourier transforms obtained (we have just shown a selection in Figs. 13 and 14) we evaluate the velocity differences between successive doublings and their ratio to see whether we can make contact with the Feigenbaum number, δ_F . Taking the velocity $v_1 = 0.23$ for the first doubling, $v_2 = 0.30$ for the second doubling and $v_3 = 0.315$ for the next element in the cascade we obtain for the ratio δ :

$$\delta = \frac{v_2 - v_1}{v_3 - v_2} = 4.67. \quad (10)$$

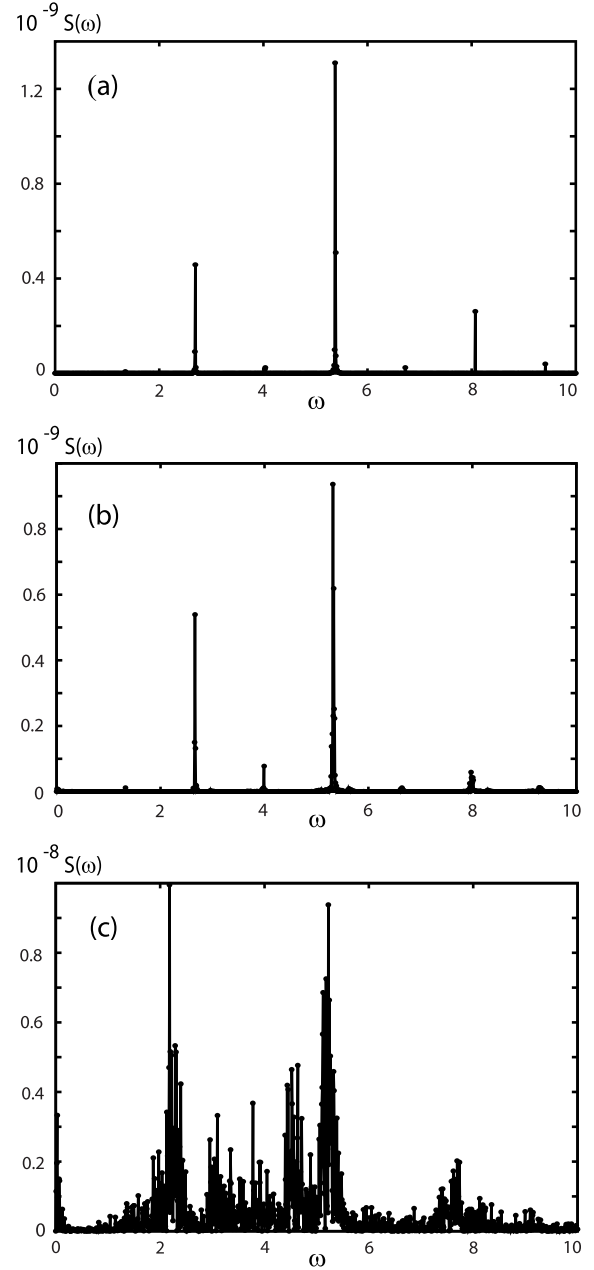


FIG. 14. In this plot we show the evolution of the Fourier transforms for larger values of the velocity, v , in the regime of oscillatory bound states for $c_r = -0.5$. (a) $v = 0.30$, a new period doubling occurs; (b) $v = 0.315$, new frequencies are starting as visible from the Fourier spectrum; (c) $v = 0.40$, fully developed chaotic state.

This value is very close to the universal Feigenbaum number $\delta_F = 4.669$. We interpret this result as an indication that a period doubling cascade is at work in our case as well thus demonstrating that a partial differential equation associated with the formation of spatially localized patterns—dissipative solitons—can show in a certain parameter regime low-dimensional behavior familiar from a class of one-dimensional maps.

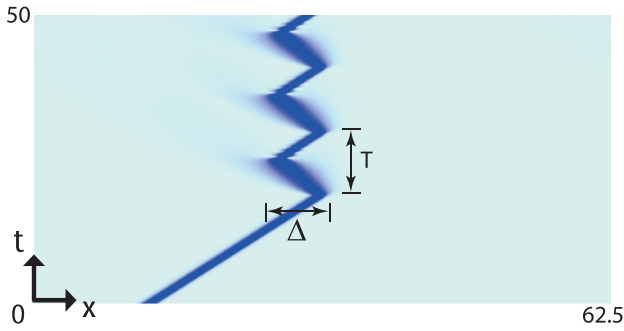


FIG. 15. Determination of period and amplitude for the large-amplitude oscillatory bound state for $c_r = -0.5$ and $v = 1.0$: $x-t$ plot showing the amplitude A of the wave traveling to the right for a shorter period of time and $L = 62.5$. For the amplitude we obtain $\Delta = 4.09$ and for the period T we get $T = 11.1$.

C. Detailed characterization of large-amplitude oscillatory bound states

One of the patterns not found before for other collisions of DSs are large-amplitude oscillatory bound states. One example of a blow-up of the general $x-t$ plot (Fig. 5) is shown in Fig. 15: The amplitude A of Fig. 5 traveling to the right on a magnified scale, which allows a precise determination of the period T and the oscillation amplitude, Δ of the large-amplitude oscillatory bound state: $T = 11.1$ and $\Delta = 4.09$. In Fig. 16 we have plotted the amplitude Δ and the period T of this pattern as a function of the velocity v . The growth rates of Δ and T as a function of velocity v closely parallel each other in their behavior but do not obey a power law or simple exponential growth. For $v = 1.26$ the two DSs annihilate, since both pulses become subcritical in size and area as $t \rightarrow T/4$.

To analyze further the data for the oscillation amplitude, Δ , and the period, T , presented in Fig. 16, we have plotted in Fig. 17 the data for the period and the rescaled data for the amplitude rescaled by a factor of $8/3$. As one can see the data almost perfectly superpose over the whole range of velocities accessible for the large-amplitude oscillatory bound state. This indicates that the two sets of data are strictly proportional to each other when considered as a function of $v - v_c$ with $v_c \approx 0.95$. From making several additional runs for c_r , we observe that the ratio Δ/T changes by less than 10% going from $c_r = -0.5$ to $c_r = -0.8$ and that it decreases slowly with decreasing c_r . Such a relationship between amplitude and period is unknown, both for linear wave equations and also for standard nonlinear prototype equations including the nonlinear Schrödinger equation and the Korteweg de Vries equation. We conclude that this direct proportionality reflects an intrinsic nonlinear property of the large-amplitude oscillatory bound state.

D. Detailed characterization of meandering oscillatory bound states and the transition to large-amplitude oscillatory bound states

Since meandering oscillatory bound states have not been described before, we describe their behavior in somewhat more detail in the following, also making use of the Fourier spectra presented in Figs. 18 and 19. As the velocity of the

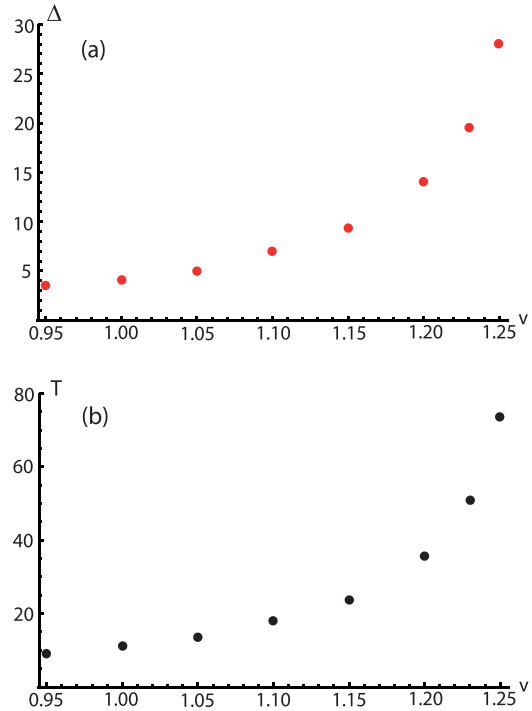


FIG. 16. Determination of amplitude Δ and period T for the large-amplitude oscillatory bound state for $c_r = -0.5$ as a function of velocity v : (a) amplitude Δ plotted as red solid circles (\bullet) as function of v ; (b) period T plotted as filled black circles (\bullet) as a function of v . In both cases we observe stronger than linear growth with growth rates that closely parallel each other. At $v = 1.26$ annihilation of the two DSs replaces large-amplitude oscillatory bound states.

colliding DSs is increased several distinct features emerge. First, the noisy background is reduced substantially with increasing velocity. Second the width of the peaks is decreasing while simultaneously their height is increasing. In addition, the number of peaks is reduced as well with growing velocity. All these properties point to a behavior, which is becoming less and less chaotic as the transition to large-amplitude

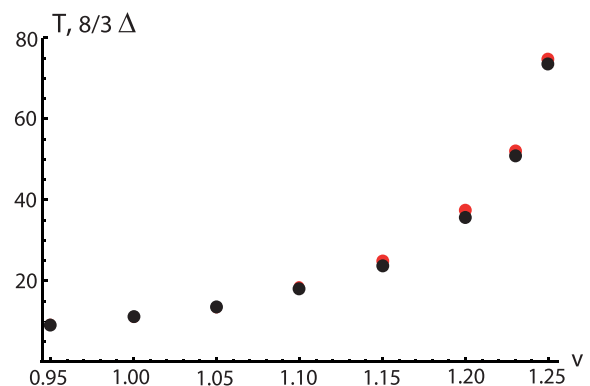


FIG. 17. The period T indicated by filled black circles (\bullet) and the rescaled amplitude, Δ (rescaled by a factor $8/3$) shown as red solid circles (\bullet) from Fig. 16 are plotted as a function of velocity v . We observe that that the curves superpose almost perfectly.

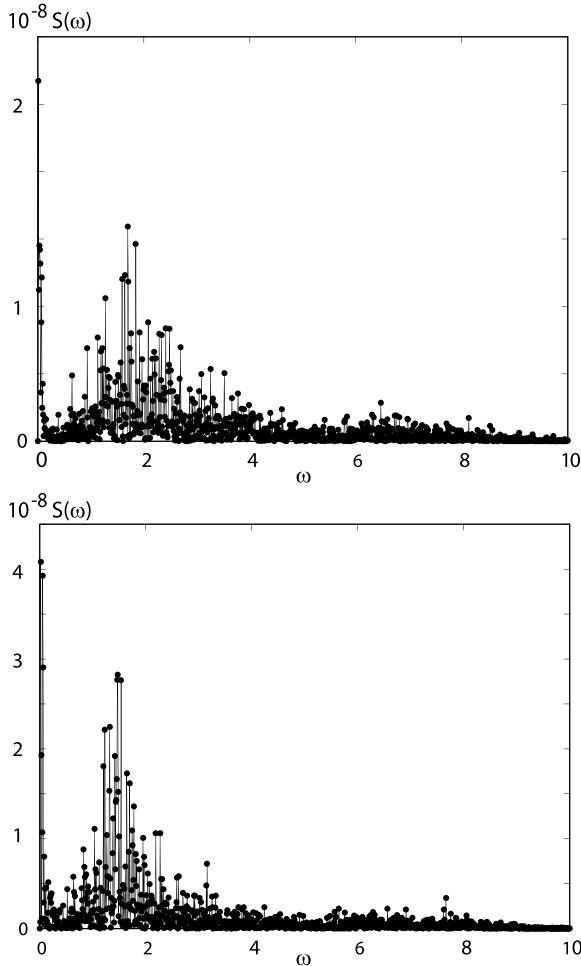


FIG. 18. The Fourier spectra for meandering oscillatory bound states for two values of the velocity v and $c_r = -0.5$. $v = 0.60$ (top) and $v = 0.70$ (bottom). The range covered for ω is $0 \leq \omega \leq 10$. While both Fourier spectra clearly showing signatures of chaotic behavior, the width of the Fourier spectrum as well as the background noise level are reduced as the velocity increases from $v = 0.60$ (top) to $v = 0.70$ (bottom).

oscillatory bound states is approached. For large-amplitude oscillatory bound states only one frequency and its harmonics are observed.

Finally, we note that within the grid spacing of the phase diagram (Fig. 1) studied here, we observed a continuous transition from meandering bound states to large-amplitude oscillatory bound states.

E. Transition to partial annihilation: Spontaneous breaking of symmetry

As we see from Fig. 1 and Fig. 9 for small negative values of the cross-coupling terms and large velocities the region of partial annihilation (only one pulse survives the collision) arises between meandering bound states and annihilation or interpenetration. Experimentally, partial annihilation has been found where also bound states appear [4,5]. Recently, in a Rapid Communication, in the framework of two coupled subcritical cubic-quintic Ginzburg-Landau equations,

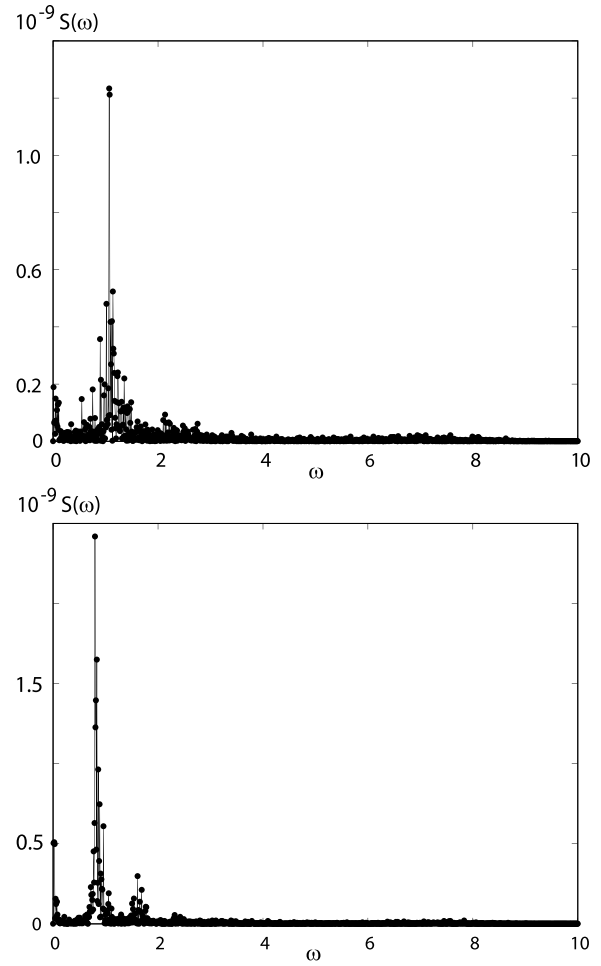


FIG. 19. The Fourier spectra for meandering oscillatory bound states for two values of the velocity v and $c_r = -0.5$. $v = 0.80$ (top) and $v = 0.90$ (bottom). The range covered for ω is $0 \leq \omega \leq 10$. We note the change in scale on the ordinate compared to Fig. 18. We note that the width of the Fourier spectrum and the background noise level are reduced as the velocity increases.

we have shown that partial annihilation arises between stationary bound states and annihilation due to spontaneously broken left-right symmetry [12]. In the same letter, briefly, we have also illustrated the case which consists of two coupled complex cubic Ginzburg-Landau equations with nonlinear gradient terms for counterpropagating waves, where partial annihilation also occurs because bound states lose their stability [12]. A big difference is that in the former case left and right partial annihilation are almost identical under reflection, whereas in the latter case there may be substantial differences.

V. CONCLUSIONS AND PERSPECTIVE

In this paper we have studied the interaction of stable DSs of the cubic complex Ginzburg-Landau equation which are stabilized only by one nonlinear gradient term, namely the Raman term. Depending on its magnitude we find up to seven possible outcomes of these collisions: Stationary bound states, oscillatory bound states, meandering oscillatory bound states, bound states with large-amplitude

oscillations, partial annihilation, complete annihilation, and interpenetration. We have analyzed meandering oscillatory bound states and bound states with large-amplitude oscillations in more detail. We find that the meandering of the meandering oscillatory bound states leads to chaotic behavior while large-amplitude oscillatory bound states are predominantly characterized by one frequency. We have compared our results with those obtained for coupled cubic-quintic complex Ginzburg-Landau equations and with the cubic-quintic complex Swift-Hohenberg equation. We conclude that both meandering oscillatory bound states as well as bound states with large-amplitude oscillations appear to be specific for coupled cubic complex Ginzburg-Landau equations with a stabilizing Raman term.

To compare with experiments we should recall that Eq. (4) has been explicitly deduced for an optical system. In this case for physical reasons, R_r must be positive. Therefore $v = v_g - v(R_r)$ will be large because $v(R_r) < 0$. Thus, it is very possible that stationary and oscillatory bound states cannot be observed, while the behaviors most likely to be observed are large-amplitude oscillatory bound states, partial annihilation, annihilation, and interpenetration.

The results described here can naturally be extended in several directions. As a next step it seems natural to discuss the influence of the other nonlinear gradient terms familiar from nonlinear optics, namely self-steepening, delayed nonlinear gain and dispersion of the nonlinear gain, since it has been shown in Ref. [29] that in several cases one nonlinear gradient term is already sufficient to stabilize the DS. Another

direction to go into will be the study of collisions of oscillatory NLGS DSs as they have been described first in Ref. [28]. We also emphasize that the study of the influence of noise on collisions will be of high interest, since it has been shown before that even small amounts of noise can qualitatively change the outcome of collisions for DSs found for the CQGL equation [11].

The most important challenge is clearly to find suitable experimental systems to study DSs stabilized exclusively by nonlinear gradient terms and their interactions. Given the nature of the gradient nonlinearities, most likely the experimental systems of choice will come from nonlinear optics.

Although experiments involving collisions in nonlinear optics are scarce, we refer to a recent article reporting explosions induced by soliton collision in a mode-locked fiber laser [7]. What we propose is to use this same medium in a collision of counterpropagating pulses with a wide spectrum (>0.1 THz) so that high-frequency components can be transferred to low-frequency ones, thus the Raman effect becomes important. For our equations to be valid it is necessary that the pulses are wide enough (~ 100 fs).

ACKNOWLEDGMENTS

O.D. and C.C. wish to acknowledge the support of FONDECYT (CL), Grant No. 1200357 and Universidad de los Andes through FAI initiatives. H.R.B. thanks the Deutsche Forschungsgemeinschaft (DE) for partial support of this work.

-
- [1] H. H. Rotermund, S. Jakubith, A. von Oertzen, and G. Ertl, *Phys. Rev. Lett.* **66**, 3083 (1991).
 - [2] A. von Oertzen, A. S. Mikhailov, H. H. Rotermund, and G. Ertl, *J. Phys. Chem. B* **102**, 4966 (1998).
 - [3] P. R. Bauer, A. Bonnefont, and K. Krischer, *Sci. Rep.* **5**, 16312 (2015).
 - [4] P. Kolodner, *Phys. Rev. A* **44**, 6448 (1991).
 - [5] P. Kolodner, *Phys. Rev. A* **44**, 6466 (1991).
 - [6] H. Kuwayama and S. Ishida, *Sci. Rep.* **3**, 2272 (2013).
 - [7] J. Peng and H. Zeng, *Commun. Phys.* **2**, 34 (2019).
 - [8] N. Akhmediev and A. Ankiewicz (eds.), *Dissipative Solitons: From Optics to Biology and Medicine* (Springer, Berlin, 2008).
 - [9] H. R. Brand and R. J. Deissler, *Phys. Rev. Lett.* **63**, 2801 (1989).
 - [10] R. J. Deissler and H. R. Brand, *Phys. Rev. Lett.* **74**, 4847 (1995).
 - [11] O. Descalzi, J. Cisternas, D. Escaff, and H. R. Brand, *Phys. Rev. Lett.* **102**, 188302 (2009).
 - [12] O. Descalzi and H. R. Brand, *Phys. Rev. E* **101**, 040201(R) (2020).
 - [13] H. R. Brand, P. S. Lomdahl, and A. C. Newell, *Phys. Lett. A* **118**, 67 (1986).
 - [14] H. R. Brand, P. S. Lomdahl, and A. C. Newell, *Physica D* **23**, 345 (1986).
 - [15] O. Thual and S. Fauve, *J. Phys. France* **49**, 1829 (1988).
 - [16] H. Sakaguchi and H. R. Brand, *Physica D* **117**, 95 (1998).
 - [17] J. Kosek and M. Marek, *Phys. Rev. Lett.* **74**, 2134 (1995).
 - [18] T. Ohta, Y. Hayase, and R. Kobayashi, *Phys. Rev. E* **54**, 6074 (1996).
 - [19] Y. Hayase and T. Ohta, *Phys. Rev. Lett.* **81**, 1726 (1998).
 - [20] M. Argentina, P. Couillet, and V. Krinsky, *J. Theor. Biol.* **205**, 47 (2000).
 - [21] M. Bar, M. Eiswirth, H. H. Rotermund, and G. Ertl, *Phys. Rev. Lett.* **69**, 945 (1992).
 - [22] R. J. Deissler and H. R. Brand, *Phys. Lett. A* **146**, 252 (1990).
 - [23] R. J. Deissler and H. R. Brand, *Phys. Rev. Lett.* **81**, 3856 (1998).
 - [24] G. P. Agrawal, *Nonlinear Fiber Optics* (Academic Press, Oxford, 2013).
 - [25] H. P. Tian, Z. H. Li, J. P. Tian, G. S. Zhou, and J. Zi, *Appl. Phys. B* **78**, 199 (2004).
 - [26] C. Cartes and O. Descalzi, *Phys. Rev. A* **93**, 031801(R) (2016).
 - [27] M. Facão and M. I. Carvalho, *Phys. Rev. E* **92**, 022922 (2015).
 - [28] M. Facão and M. I. Carvalho, *Phys. Rev. E* **96**, 042220 (2017).
 - [29] M. I. Carvalho and M. Facão, *Phys. Rev. E* **100**, 032222 (2019).
 - [30] I. S. Aranson and L. Kramer, *Rev. Mod. Phys.* **74**, 99 (2002).
 - [31] H. R. Brand and R. J. Deissler, *Phys. Rev. Lett.* **63**, 508 (1989).
 - [32] H. R. Brand and R. J. Deissler, *Phys. Rev. A* **41**, 5478 (1990).
 - [33] R. J. Deissler, Y. C. Lee, and H. R. Brand, *Phys. Rev. A* **42**, 2101 (1990).
 - [34] H. Sakaguchi, *Prog. Theor. Phys.* **87**, 1049 (1992).
 - [35] H. Sakaguchi, *Prog. Theor. Phys.* **89**, 1123 (1993).
 - [36] H. Sakaguchi and H. R. Brand, *Physica D* **97**, 274 (1996).
 - [37] O. Descalzi, J. Cisternas, and H. R. Brand, *Phys. Rev. E* **100**, 052218 (2019).
 - [38] O. Descalzi and H. R. Brand, *Chaos* **30**, 043119 (2020).
 - [39] O. Descalzi, J. Cisternas, and H. R. Brand, *Phys. Rev. E* **74**, 065201(R) (2006).
 - [40] O. Descalzi, J. Cisternas, P. Gutiérrez, and H. R. Brand, *Eur. Phys. J. Spec. Top.* **146**, 63 (2007).